RESEARCH

Enhancement of ruthenium-promoted Co/CNTs nanocatalyst performance using microemulsion technique

Ahmad Tavasoli · Somayeh Taghavi · Saber Tabyar · Saba Karimi

Abstract

Background Ruthenium-promoted cobalt nanocatalysts that are supported by carbon nanotubes (CNTs) are prepared using impregnation and microemulsion techniques. Ruthenium loadings were varied from 0 to 1 wt% while the amount of cobalt was fixed at 15 wt%. The nanocatalysts were extensively characterized by different methods and their activity and selectivity in Fischer–Tropsch synthesis (FTS) have been assessed in a fixed-bed microreactor. The physicochemical properties and performance of the nanocatalysts were compared with the catalyst prepared by impregnation method.

Results Very narrow particle size distribution has been produced by the microemulsion technique. According to the transmission electron microscopy, pictures small Co particles (2–7 nm) are mostly confined inside the CNTs. Ruthenium increased the percentage reduction of the unpromoted catalyst by a factor of 25. Compared with the catalysts prepared by impregnation, using microemulsion technique with water-to-surfactant ratio of 0.5 which decreased the average cobalt oxide particle sizes to 4.8 nm, the percentage of dispersion is almost doubled and the percentage of reduction is increased by 28.

Conclusions Addition of ruthenium increased the percentage conversion and C_5^+ selectivity of the unpromoted catalyst by a factor of 22.6 and 7, respectively. Activity and selectivity were found to be dependent on the catalyst preparation method and water-to-surfactant ratio (as well as on cobalt particle sizes). The percentage of CO conversion and FTS rate increased from 59.09 to 75.05 and 0.291 to 0.372 g HC/g cat/h, respectively, while the C_5^+ liquid hydrocarbons selectivity decreased slightly.

A. Tavasoli (✉) · S. Taghavi · S. Tabyar · S. Karimi
School of Chemistry, College of Science, University of Tehran, Tehran 1513746911, Iran
e-mail: tavassolia@khayam.ut.ac.ir

Introduction

Fischer–Tropsch synthesis (FTS) is an alternative route for the production of transportation fuels from natural gas. Regardless of the operating conditions, FTS always produces a wide range of light gases and distillates, including olefins, paraffins and oxygenated products. Cobalt-based catalysts are preferentially applied in FTS processes aimed at producing precursors of the synthetic diesel owing to their high selectivity toward long-chain normal paraffins, their remarkable stability and their lower activity for the competing water gas shift reaction (WGSR) as compared to alternative catalysts based on iron [1–3].

For cobalt catalysts supported on Al_2O_3, SiO_2 and TiO_2 it has been shown that, noble metals such as ruthenium are typically used to decrease the reduction temperature of the cobalt oxides and increase the dispersion of the cobalt clusters. Ru increases the number of active surface Co^o sites available for FTS reaction in Ru-promoted catalysts and hence enhances the percentage of CO conversion and FTS reaction rate. Ru is more selective toward higher molecular weight hydrocarbons than cobalt. Therefore, the improvement in C_5^+ selectivity observed for Ru-promoted catalysts as compared to unpromoted catalyst may be due to the Ru enrichment on the cobalt crystallite surface [4, 5].

One of the important factors in catalyst activity and product selectivity is the catalyst preparation method. The synthesis of inorganic nanoparticles is usually carried out in water-in-oil (*W/O*) microemulsions which consist of small aggregates (micelles) at the microscopic level. *W/O* microemulsion solutions are mostly transparent, isotropic

Springer

liquid media with nanosized water droplets that are dispersed in the continuous oil phase and stabilized by surfactant molecules at the water/oil interface. These surfactant-covered water pools offer a unique microenvironment for the formation of nanoparticles. In the catalysts prepared by impregnation technique, the structure of the support, especially the pore size, influences the sizes of the formed metal particles with a broad size distribution, while in the catalysts prepared by the microemulsion route the sizes of the particles will depend on the nature of the microemulsion. In this case, a narrow particle size distribution can be obtained. The main advantages of using the microemulsion technique in the preparation of catalysts is the possibility of controlling properties such as particle size, morphology and size distribution. Moreover, with the microemulsion method it is possible to control the composition of the nanoparticles such as bimetallic particles, where the initial ratio of the metal precursor concentrations in the water cores of the micelles will correspond to the final composition of the particles obtained after reduction. Using microemulsion, the bimetallic particle can be formed at room temperature with a true alloy structure while conventional preparation methods usually require high temperatures which inherently will cause formation of large particles [6–8].

In cobalt-catalyzed FTS, to achieve high surface active sites (Co^o), cobalt precursors are dispersed on porous carriers such as SiO$_2$, Al$_2$O$_3$ and to a lesser extent TiO$_2$ [9–16]. In our previous works, we showed that a negative aspect of these support materials is their reactivity toward cobalt, which during preparation or catalysis results in the formation of mixed compounds that are reducible only at high reduction temperatures [17, 19]. To avoid these problems, we used the CNTs as FTS catalyst support [4, 17–19]. We showed that using CNTs can increase the dispersion of metal clusters and decrease the average cobalt clusters sizes, which in turn can enhance the catalyst performance [18, 19]. In the mentioned works, we used impregnation method to prepare the CNTs supported cobalt catalysts. In the present work, we intend to use the bimetallic microemulsion technique for preparation of ruthenium-promoted cobalt catalyst. Also, the influences of cobalt particle size on the catalyst physicochemical properties, activity and selectivity were assessed and reported.

Results and discussion

Catalysts characterization

Textural properties of the fresh and purified CNTs are given in the Table 1. The data indicate that in the case of acid-washed support, surface area, total pore volume and average

Table 1 Textural properties of the fresh and purified carbon nanotubes

Sample	BET surface area (m^2/g)	Total pore volume (ml/g)	Average pore diameter (Å)	% Metal
Fresh CNTs	209	0.48	91.62	0.60
Treated CNTs	252.6	0.59	94.12	0

BET Brunauer, Emmett, and Teller

internal diameter of nanotubes increased significantly which will result in better dispersion of metals as well as enhancement of catalyst activity. Table 1 also shows the Fe content for the untreated fresh CNTs and acid-treated CNTs (determined by ICP). As shown the amount of encapsulated Fe content in the fresh CNTs was about 0.6 wt% which decreased to zero for acid-treated CNTs.

Results of surface area measurements for the calcined catalysts are given in the Table 2. These results show that the BET surface areas of the C$_4$–C$_8$ (prepared by microemulsion) catalysts range from 187 to 169 m^2/g. However, the BET surface area for the C$_1$–C$_3$ catalysts (prepared by impregnation) is somewhat lower (154–158 m^2/g), which indicates some more pore blockage by metal oxide clusters in the catalysts prepared by impregnation method than the catalysts prepared by microemulsion method. This table also shows that the BET surface area of the catalysts prepared by micro emulsion increases by decreasing the W/S ratio indicating smaller cobalt particles and lesser pore blockage by cobalt oxide clusters.

The elemental compositions of the calcined catalysts measured by ICP are given in Table 3. This table shows that the metal contents of the catalysts were fairly similar and close to the targeted metal contents.

Figure 1 presents the TEM image of the purified support. As shown the treated support is comprised of an interwoven matrix of multiwall carcon nanotubes. TEM images of C$_4$ catalyst made by the microemulsion method, are shown in Fig. 2. As shown, the very small particles are dispersed mostly inside the tubes and on the outer surface of the CNTs walls. The size of the particles located inside and outside the nanotubes are within the range of 2–7 nm. The TEM image of C$_3$ catalyst prepared by impregnation method is shown in Fig. 3. This figure shows that the particles are distributed both inside and outside of the nanotubes walls. The size of particles located inside and outside the nanotubes is within the range of 4–16 nm.
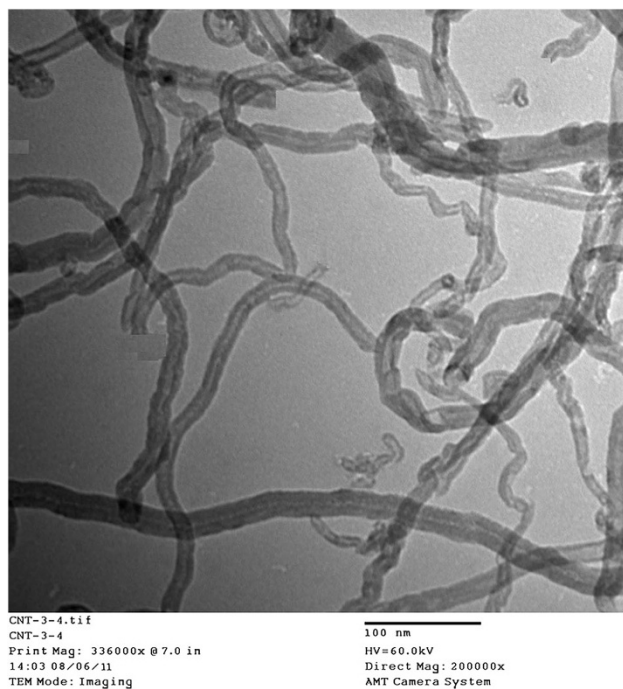
Figure 4 depicts the size distribution of the particles for C$_3$ and C$_6$ catalysts, which is determined using the population of the total particles of the catalyst based on data taken from 5 TEM pictures. According to this figure, the average particle size for the C$_3$ and C$_4$ catalysts are 4.7 and

Table 2 Textural properties of the calcined catalysts with different preparation methods

Sample	Preparation route	Co wt%	Ru wt%	W/S ratio	BET surface area (m²/g)	Total pore volume (ml/g)	Average pore diameter (Å)
C_1	Impregnation	15	0.0	–	158	0.438	128
C_2	Impregnation	15	0.5	–	156	0.435	129
C_3	Impregnation	15	1.0	–	154	0.432	130
C_4	Microemulsion	15	1.0	0.50	187	0.469	125
C_5	Microemulsion	15	1.0	0.75	180	0.461	127
C_6	Microemulsion	15	1.0	1.0	174	0.453	127
C_7	Microemulsion	15	1.0	1.25	172	0.447	129
C_8	Microemulsion	15	1.0	1.50	169	0.443	129

Table 3 Chemical composition of the calcined catalysts

Catalyst	Targeted composition (wt%)		Measured composition (wt%)	
	Co	Ru	Co	Ru
C_1	15	0.0	14.69	0.0
C_2	15	0.5	14.68	0.049
C_3	15	1	14.68	0.979
C_4	15	1	14.37	0.958
C_5	15	1	14.40	0.960
C_6	15	1	14.41	0.961
C_7	15	1	14.41	0.961
C_8	15	1	14.43	0.962

15 Co-11.tif
15 Co-11
Print Mag: 577000x @ 8.0 in
11:12 08/06/11
TEM Mode: Imaging

20 nm
HV=60.0kV
Direct Mag: 300000x
AMT Camera System

Fig. 2 TEM image of the C_4 catalyst (prepared by microemulsion and W/S = 0.5)

CNT-3-4.tif
CNT-3-4
Print Mag: 336000x @ 7.0 in
14:03 08/06/11
TEM Mode: Imaging

100 nm
HV=60.0kV
Direct Mag: 200000x
AMT Camera System

Fig. 1 TEM image of the purified CNTs

8.4 nm, respectively. Of particular importance, the particle size distribution is too narrow in the case of C_3, the catalyst prepared by microemulsion method.

To determine the crystalline phases, X-ray diffraction experiments (XRD) of the calcined catalysts were performed. XRD patterns of the catalysts are shown in Fig. 5a, b. In the XRD spectra of all the catalysts, the peaks at 2θ values of 25° and 43° correspond to the support, while the other peaks in the spectra of the catalysts are related to different crystal planes of Co_3O_4 [18, 19]. The peak at 36.8° is the most intense peak of Co_3O_4 in XRD spectrum
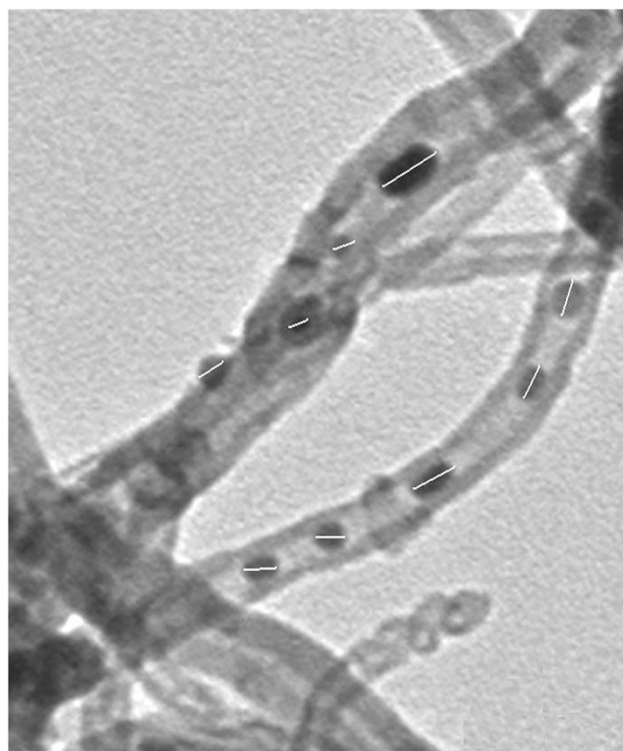
15 Co-12.tif
15 Co-12
Print Mag: 577000x @ 8.0 in
12:31 08/06/11
TEM Mode: Imaging

20 nm
HV=60.0kV
Direct Mag: 300000x
AMT Camera System

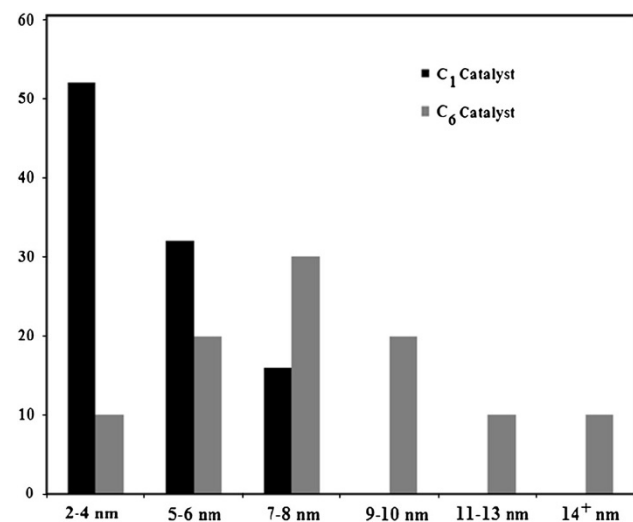Fig. 3 TEM image of the C_3 catalyst (prepared by impregnation)

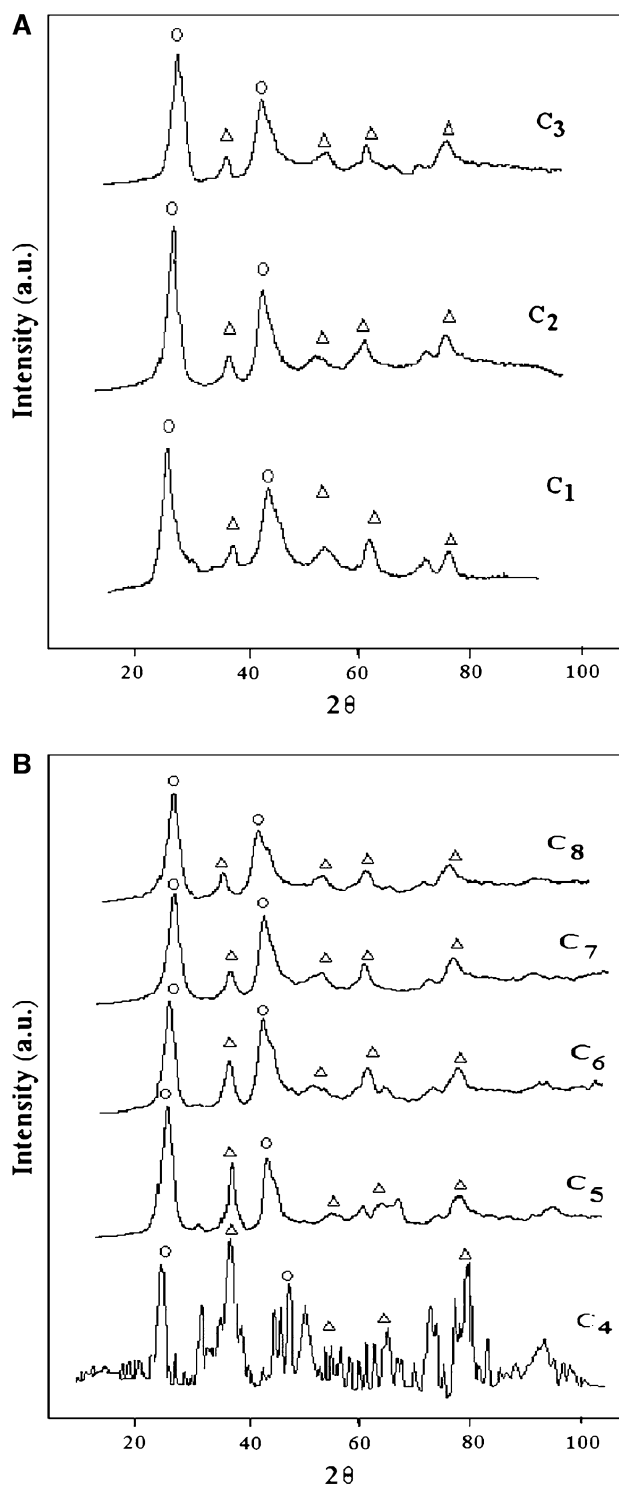Fig. 4 Particle size distributions for the C_3 and C_4 catalysts

Fig. 5 X-ray diffraction (XRD) of the catalysts prepared using different methods. **a** Impregnation method. **b** Microemulsion method. *Open circle* CNTs, *open triangles* cobalt oxides

of all the catalysts. Due to the low amounts of Ru promoter, in the XRD spectrum of the catalysts, no peak is observed in Fig. 5a, b indicating diffraction lines of ruthenium oxide. Table 4 shows the average Co_3O_4 cluster size of the

catalysts calculated from XRD spectrum and Scherer equation at 36.8° [19]. According to Table 4, the average Co_3O_4 cluster size for the catalysts synthesized by microemulsion is significantly lower compared to the catalysts

Table 4 Particle sizes of the calcined catalysts with different preparation methods

Catalyst	d (Co_3O_4) (nm) calculated by Debye–Scherer formula
C_1	8.5
C_2	8.6
C_3	8.7
C_4	4.8
C_5	5.0
C_6	5.3
C_7	5.7
C_8	7.2

prepared by impregnation method, indicating better dispersion of cobalt clusters. Also, in the case of the catalysts prepared by microemulsion, the average Co_3O_4 cluster size was decreased from 7.2 to 4.8 nm by decreasing the W/S ratio from 1.5 to 0.5. The average particle sizes of Co_3O_4 are linearly correlated with the water-to-surfactant ratio used during the microemulsion catalyst preparation route. In fact, nanoparticles are formed in the internal structure of the microemulsion, which is determined by the water-to-surfactant ratio. At high oil concentration, the bicontinuous phase is transformed into a structure of small water droplets within a continuous oil phase (reverse micelles) when surfactant is added. Thus, the results show that the size of different droplets determines the cobalt's particle size, depending on the amount of surfactant [6–8].

The activation of the catalysts in hydrogen atmosphere was disclosed by temperature-programmed reduction (TPR) experiments. The TPR spectra of the calcined catalysts are shown in Fig. 6a, b. In the TPR profile of all the catalysts, the low temperature peak is typically assigned to reduction of Co_3O_4 to CoO, although a fraction of the peak likely comprises the reduction of the larger bulk-like CoO species to Co^o [18, 19]. The second broad peak is assigned to reduction of small CoO to Co^o species. Figure 6a shows that addition of Ru to the Co/CNTs catalyst decreases the reduction temperature of cobalt oxides, significantly. Ruthenium oxide reduces at temperatures lower than the reduction temperature of Co_3O_4 which in turn enhances the reduction of cobalt oxides by spillover of hydrogen. Figure 6b shows that deposition of cobalt nanoparticles synthesized by microemulsion on the CNTs shifts the reduction peaks of the Co_3O_4 to CoO and the CoO to Co^o species to the lower temperatures compared to the catalyst prepared by impregnation method with the same loadings of Co and Ru. Also, for the catalysts prepared by microemulsion, decreasing water-to-surfactant ratio shifts the reduction of the Co_3O_4 to CoO and the CoO to Co^o species to the lower temperatures, indicating higher reducibility for the catalysts prepared with lower W/S ratios. As confirmed by XRD and
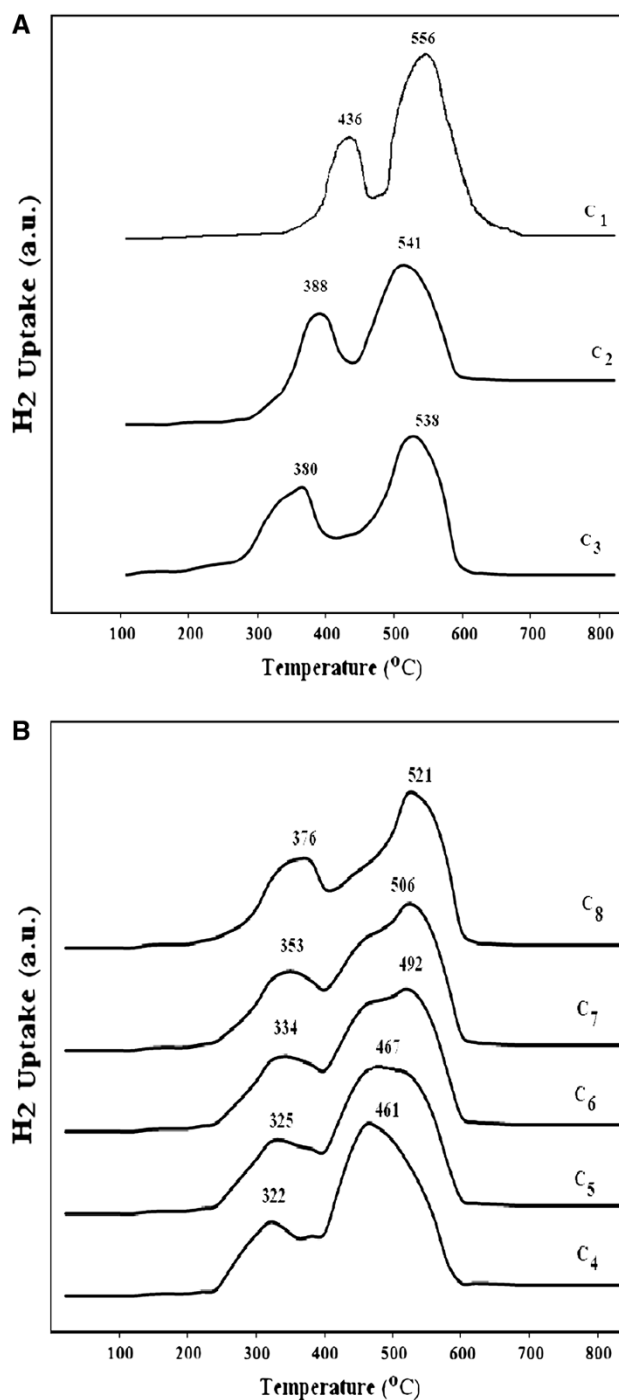
Fig. 6 TPR of the calcined catalysts prepared using different methods. **a** Impregnation. **b** Microemulsion

TEM tests, using microemulsion technique at lower W/S ratios decreases the cobalt average particle sizes which in turn increases the population of the particles located inside the CNTs. Positioning the cobalt particles inside the nanotubes favors the reduction of Co_3O_4 and CoO species. The electron deficiency of the interior CNTs surface is possibly responsible, because the π electron density of the graphene

layers shifts from the inner to outer surface of the CNTs. Thus, Co_3O_4 should interact with the interior CNTs wall differently from that with the exterior wall. This is reflected by the shift of the Co–O vibration mode when Co_3O_4 nanoparticles are moved from the outside to the inside of the CNTs channels. Within the channels, the electron density loss can be at least partially compensated through this interaction with the encapsulated Co_3O_4, which can destabilize Co_3O_4 and results in an easier reduction. Higher degree of reduction in the case of the catalysts prepared by microemulsion with lower W/S ratios will make more cobalt atoms to be available for FTS reaction. Figure 6a, b also indicates that there is no significant evidence of formation of metal-supported compounds on the catalyst surface due to the absence of significant reduction peaks above 580 °C. It has been shown that the reduction peaks present at temperatures above 580 °C with oxidic carrier show formation of cobalt species that are difficult to reduce (oxide compounds). CNTs as an inert support for cobalt catalyst do not show any peak related to formation of metal-support compounds as compared to Co/γ-Al_2O_3 catalysts suggesting an easier reduction process with CNTs than with oxidic carriers [17, 20].

The results of hydrogen chemisorption tests are given in Table 5. As shown, addition of Ru to the unpromoted Co/CNTs catalyst increases the hydrogen uptake, percentage reduction and percentage dispersion. Table 5 also shows that, using microemulsion considerably increased the hydrogen uptake and percentage dispersion. For the catalysts prepared with microemulsion method, in accordance with the results of TPR tests, hydrogen uptake and percentage dispersion increased with decreasing W/S ratio. Maximum dispersion is achieved at the minimum W/S ratio of 0.5. The average particle diameter decreased, which is in

agreement with the results of XRD and TEM tests. Also, the percentage reduction of the catalysts shows a considerable increase. Higher dispersions and smaller cobalt cluster sizes in the case of the catalysts prepared by microemulsion will increase the number of sites available for CO conversion and hydrocarbon formation reaction rates.

Activity and product selectivity for FTS

The performances of all the catalysts in the FTS were tested in a fixed-bed micro-reactor. All the reactions were performed under a set of standard conditions (220 °C, 2 MPa, H_2:CO = 2). The catalysts reached their normal activity within 24 h. Table 6 presents the FTS rate (g CH/g cat/h), percentage of CO conversion and different product selectivities of the C_4 (prepared by microemulsion 15 wt% Co and 1 wt% of Ru) and C_3 (prepared by impregnation 15 wt% Co and 1 wt% of Ru) catalysts during the first 24 h of FTS. As shown in Table 6, the FTS productivity of the C_4 catalyst (0.372 g CH/g cat/h) is significantly greater than that of the C_3 catalyst (0.291 g CH/g cat/h). Several reasons can be associated with the improvement in FTS productivity of C_4 catalyst. TEM, XRD and H_2 chemisorption results showed that the average size of the particles for C_4 and C_3 catalysts was about 4.8 and 8.7 nm, respectively. Lower particle sizes in the case of C_4 catalyst increase the active metal surface area which in turn leads to higher FTS rate. As discussed earlier, H_2-TPR analysis revealed that the reducibility of the C_3 catalyst was higher compared with the C_4. This phenomenon can result in the formation of more catalytically active sites for FTS. So in industrial scale, using microemulsion method for preparation of FTS catalysts, with higher volumetric productivity, will decrease reactor volume requirements and as a result

Table 5 H_2 chemisorption results for the calcined catalysts with different preparation methods

Catalyst	μ mole H_2 desorbed/g cat	μ mole O_2 Consumed/g cat	% Red.	% Dispersion	d (Co_3O_4) (nm)	d (Co^o) (nm)
C_1	210	697	36.1	13.45	8.1	6.1
C_2	220	840	43.6	14.10	8.3	6.2
C_3	226	865	44.9	14.50	8.5	6.4
C_4	393	1,265	65.7	26.75	4.6	3.5
C_5	374	1,195	62.1	25.30	4.9	3.7
C_6	339	1,127	58.5	22.80	5.4	4.1
C_7	312	1,040	54.0	20.50	5.9	4.4
C_8	259	921	47.8	16.60	7.1	5.3

Table 6 FTS results during first 24 h for the C_3 and C_4 catalysts

Catalyst	Percentage of CO Conversion	FTS rate (g CH/g cat/h)	CO_2 selectivity	CH_4 selectivity	C_2–C_4 selectivity	C_5^+ selectivity
C_4	75.05	0.372	0.510	7.97	3.91	87.61
C_3	59.09	0.291	0.51	4.68	2.43	92.38

the capital cost of the plant as compared to the catalysts prepared by impregnation.

Also the product distribution of C_4 catalyst shows a slight shift to the lower molecular weight hydrocarbons. The data show that CH_4 and light gaseous hydrocarbons selectivities of the C_4 catalyst are about 37.7 % higher than that of the C_3 catalyst. Also C_5^+ selectivity of the C_4 is about 5.44 % lower than that of the C_3. CO_2 selectivities of the C_3 and C_4 catalysts are comparable, indicating similar water gas shift activity for both catalysts. It seems that, confinement of the cobalt particles inside the pores in the case of C_3 catalyst can restrain the growth of longer chain hydrocarbons. The inner sides of the CNTs are electron-deficient and can restrain the dissociative adsorption of CO and readsorption of olefins resulting in production of lower chain hydrocarbons for C_3 catalyst. The result of Table 6 shows that C_4-catalyzed FTS is advantageous in carbon utilization as compared to processes using C_3 catalyst. It worthy is to note that, the microemulsion preparation method is more expensive than the impregnation method.

Figure 7 shows the variations of percentage of CO conversion and the number of active cobalt sites with water-to-surfactant ratio for the catalysts prepared by impregnation and different amounts of Ru. The number of active cobalt sites was defined as:

No. act. site = Wt. of Co × red. frac. × Dis. × N_A × MW,

where N_A is Avogadro's number and MW is molecular weight of cobalt. As shown in this figure, addition of Ru to the unpromoted cobalt catalyst increases the number of active cobalt sites as well as the percentage CO conversion. The trend for the percentage of CO conversion is similar to
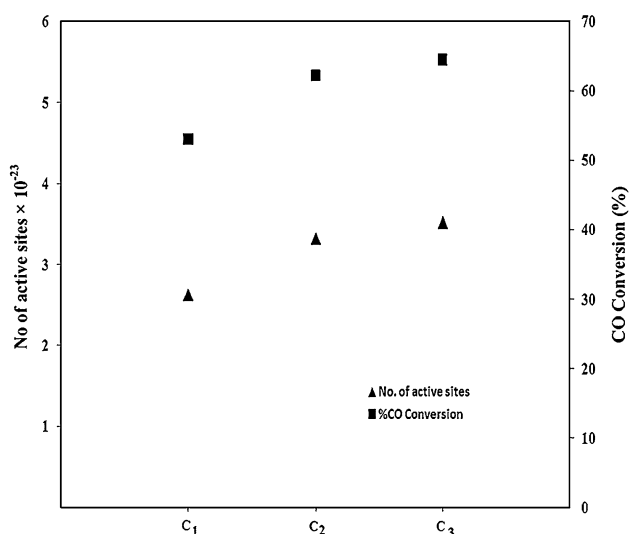
that for the number of active cobalt sites. The percentage of CO conversion increases in accordance with the number of active cobalt sites. The maximum FTS activity is achieved with the maximum amount of Ru and highest number of active cobalt sites. TPR and H_2 chemisorption tests showed that addition of Ru to the unpromoted cobalt catalyst increases the percentage reduction of the catalyst. This figure reveals that the Fischer–Tropsch activity is strongly proportional to the number of surface-reduced cobalt sites. Therefore, the maximum concentration of surface Co^o sites and FTS activity is achieved for the C_3 catalyst presenting the highest dispersion and highest reducibility. Figure 8 shows the methane, light gaseous hydrocarbons and C_5^+ selectivities of the C_1–C_3 catalysts. As shown, the methane and light gaseous hydrocarbons selectivities are reduced with increasing Ru. The catalyst prepared with 1 wt% of Ru showed lowest selectivity to methane. The C_5^+ selectivity is increased with increasing Ru. Ruthenium enriches on the surface and since Ru is the most selective FTS catalyst toward higher molecular weight hydrocarbons, enhances the selectivity of unpromoted Co/CNTs toward higher molecular weight hydrocarbons.

Figure 9 shows the variations of percentage of CO conversion and the number of active cobalt sites with water-to-surfactant ratio for the catalysts prepared by microemulsion. This figure also reveals that increasing the water-to-surfactant ratio decreases the number of active cobalt sites. The trend for the percentage of CO conversion is similar to that for the number of active cobalt sites. The percentage of CO conversion decreases in accordance with the number of active cobalt sites. The maximum FTS activity is achieved with the minimum W/S ratio and
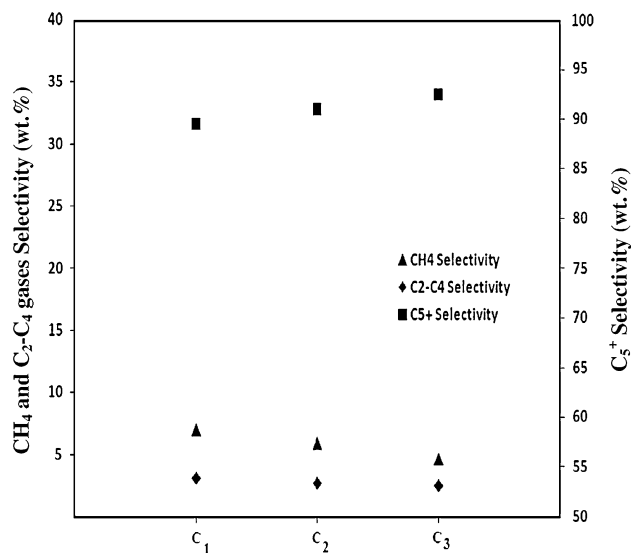

Fig. 7 Variations of percentage of CO conversion and number of active cobalt sites for the catalyst prepared with impregnation

Fig. 8 Variations of CH_4, C_2–C_4 and C_5^+ selectivities with for the catalyst prepared with impregnation
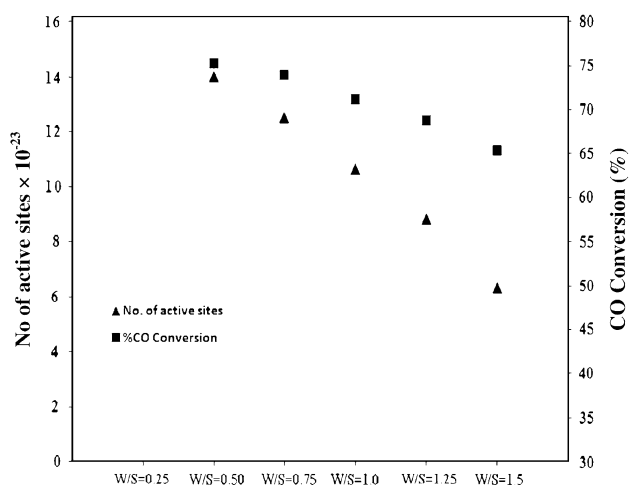
Fig. 9 Variations of percentage of CO conversion and number of active cobalt sites with water-to-surfactant ratio
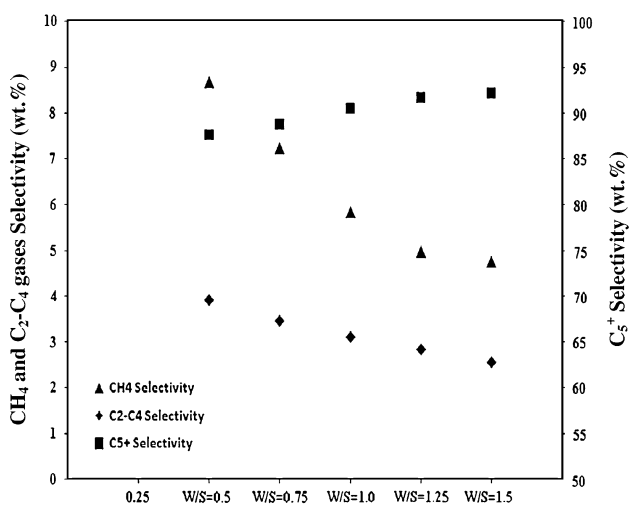

Fig. 10 Variations of CH_4, C_2–C_4 and C_5^+ selectivities with water-to-surfactant ratio

highest number of active cobalt sites. This figure reveals that the Fischer–Tropsch activity is strongly proportional to the number of surface-reduced cobalt sites. Therefore, the maximum concentration of surface Co^o sites and FTS activity is achieved for the C_4 catalyst presenting the lowest average cobalt particle sizes, best dispersion and highest reducibility. Also, improvement of the uniformity of the catalyst particles by decreasing the W/S ratio, leads to a better stability of the products and the FTS activity.

Figure 10 shows the methane, light gaseous hydrocarbons and C_5^+ selectivities of the catalysts with variation of W/S ratio. As shown, the methane and light gaseous hydrocarbons selectivities are reduced with increasing W/S ratio. The catalyst prepared with W/S of 1.5 showed lowest selectivity to methane. The C_5^+ selectivity is increased

with increasing W/S ratio. The Anderson–Schultz–Florey (ASF) model is a common model used to describe the chain growth mechanism in FTS. According to this model, the polymerization process in FTS is assumed to initiate on the surface of the catalyst by a monomer that contains one carbon atom. Chain growth takes place by the addition of monomers to the growing chains. It seems that the steric hindrance for dissociative adsorption of CO and formation of $-CH_2-$ monomer and addition of this monomer to the growing chain is less in the larger cobalt clusters which are formed at low W/S ratios.

Experimental

Catalyst preparation

Multiwall carcon nanotubes CNTs (Characteristics are shown in Table 1) were used as support for preparation of the catalysts. Prior to catalyst preparation, the support was treated with 30 % HNO_3 refluxed at 120 °C overnight, washed with distilled water several times and dried at 120 °C for 6 h. Two different sets of catalysts were prepared by microemulsion and impregnation methods. For the first set of the catalysts, the concentration of cobalt was adjusted at 15 wt% and the concentrations of ruthenium were adjusted at 0.0, 0.5 and 1.0 wt%. The catalysts were prepared by the co-impregnation method using aqueous solutions of $CO(NO_3)_2 \cdot 6H_2O$ and $Ru(NO)(NO_3)_3$. After the impregnation step, the catalysts were dried at 120 °C and calcined at 450 °C under Argon flow for 3 h and slowly exposed to an oxygen atmosphere during the cooling step. The catalysts prepared by this procedure were signified as C_1, C_2 and C_3 (see Table 2).

For the second set of the catalysts, the concentrations of cobalt and ruthenium were fixed at 15 and 1 wt%, respectively. The catalysts were prepared by microemulsion technique with aqueous solutions of cobalt nitrate $(CO(NO_3)_2 \cdot 6H_2O$ %99, Merck) and ruthenium nitrosyl nitrate $(Ru(NO)(NO_3)_3$, Aldrich). Ruthenium-promoted cobalt nanoparticles were synthesized in a reverse microemulsion using a nonionic surfactant Triton X-100 (Chem-Lab), n-hexane $(C_6H_{14}$, Chem-Lab) as the oil phase and 1-Butanol $(C_4H_9OH$, Merck) as the co-surfactant. The water-to-surfactant molar ratio (W/S) was varied from 0.5 to 1.5. After vigorous stirring, a microemulsion was obtained (15 min). Hydrazine was added in excess (Hydrazine/Co = 10) to improve nanoparticle formation in the core of the micelles by reducing the metal oxides. Then, the appropriate weight of purified CNTs was added under stirring. During the 3 h of stirring, tetrahydrofuran (THF), an emulsion destabilizing agent, was added drop wise (1 ml/min). A fast addition could lead to fast particle

agglomeration and uncontrolled particle deposition on the support (CNTs). The mixture was left to mature and settle slowly overnight and then decanted. The solid sample was recovered by vacuum filtration using ash less filtration paper (Whatman1) and washed several times with distilled water ethanol. To remove the remaining traces of surfactant and ammonia, the catalysts were dried at 120 °C for 2 h and calcined under argon (Ar) flow at 450 °C for 3 h and slowly exposed to an oxygen atmosphere during the cooling step. The catalysts prepared by this procedure were signified as C_4, C_5, C_6, C_7 and C_8 for a *W/S* ratio of 0.50, 0.75, 1, 1.25 and 1.50, respectively (see Table 2).

Inductively coupled plasma-optical emission spectrometry

The metal loadings of the calcined catalysts were performed using Varian VISTA-MPX inductively coupled plasma-optical emission spectrometry (ICP-OES) instrument (Varian Medical Systems, Inc., Palo Alto, CA,USA).

BET surface area measurements/BJH pore size distributions

Surface area, pore volume and pore average diameter of the calcined catalysts were measured using an ASAP-2010 V2 Micrometrics system (Micromeritics Instrument Corp., Norcross, GA, USA). The samples were degassed at 200 °C for 4 h under 50 mTorr vacuums and their Brunauer, Emmett, and Teller (BET) area, pore volume and pore diameter were determined.

Transmission electron microscopy (TEM)

The morphology of the treated CNTs and C_3 and C_4 catalyst was studied by TEM. Sample specimens for TEM studies were prepared by ultrasonic dispersion of the catalysts in ethanol, and the suspensions were dropped onto a carbon-coated copper grid. TEM investigations were carried out using a Philips CM20 (100 kV) transmission electron microscope equipped with a NARON energy-dispersive spectrometer with a germanium detector (Philips, Amsterdam, The Netherlands).

X-ray diffraction

The phases and particle sizes of the crystals present in the catalysts were analyzed by XRD using a Philips Analytical X-ray diffractometer (XPert MPD) with monochromatized Cu/Kα radiation, 2θ angles from 20° to 80°. The Debye–Scherer formula was applied to Co_3O_4 peaks at $2\theta = 36.8$, to calculate the average particle sizes.

Temperature-programmed reduction

The H_2-TPR profiles of the catalysts were performed to study the reducibility of the metal species in the catalysts. The calcined catalyst sample (0.05 g) was first purged in a flow of Helium at 140 °C to remove traces of water and gases exist in catalyst, and then cooled to 40 °C. Then the TPR of each sample was performed using 5 % H_2 in Ar stream at a flow rate of 40 ml/min at atmospheric pressure using Micrometrics TPD–TPR 2900 analyzer equipped with a thermal conductivity detector (TCD), heating at a linearly programmed rate of 10 °C/min up to 850 °C.

Hydrogen chemisorption

The amount of chemisorbed hydrogen on the catalysts was measured using the Micromeritics TPD–TPR 290 system. 0.25 g of the sample was reduced under hydrogen flow at 400 °C for 12 h and then cooled to 100 °C under hydrogen flow. Then the flow of hydrogen was switched to argon at the same temperature, which lasted about 30 min to remove the weakly adsorbed hydrogen. Afterwards, the temperature-programmed desorption (TPD) of the samples was obtained by increasing the temperature of the samples, with a ramp rate of 10 °C/min, to 400 °C under the argon flow. The TPD profile was used to determine the cobalt dispersion and its surface average crystallite size. After the TPD of hydrogen, the sample was reoxidized at 400 °C by pulses of 10 % oxygen in helium to determine the extent of reduction. It is assumed that Co^o is oxidized to Co_3O_4. The calculations are summarized below.

$$\text{Calibration value (1 gas/area units)}$$
$$= \frac{\text{Loop volume} \times \%\text{Analytical gas}}{\text{Mean calibration area} \times 100} \tag{1}$$

$$H_2 \text{ uptake (moles/g}_{cat})$$
$$= \frac{\text{Analytical area from TPD} \times \text{Calibration value}}{\text{Sample weight} \times 24.5} \tag{2}$$
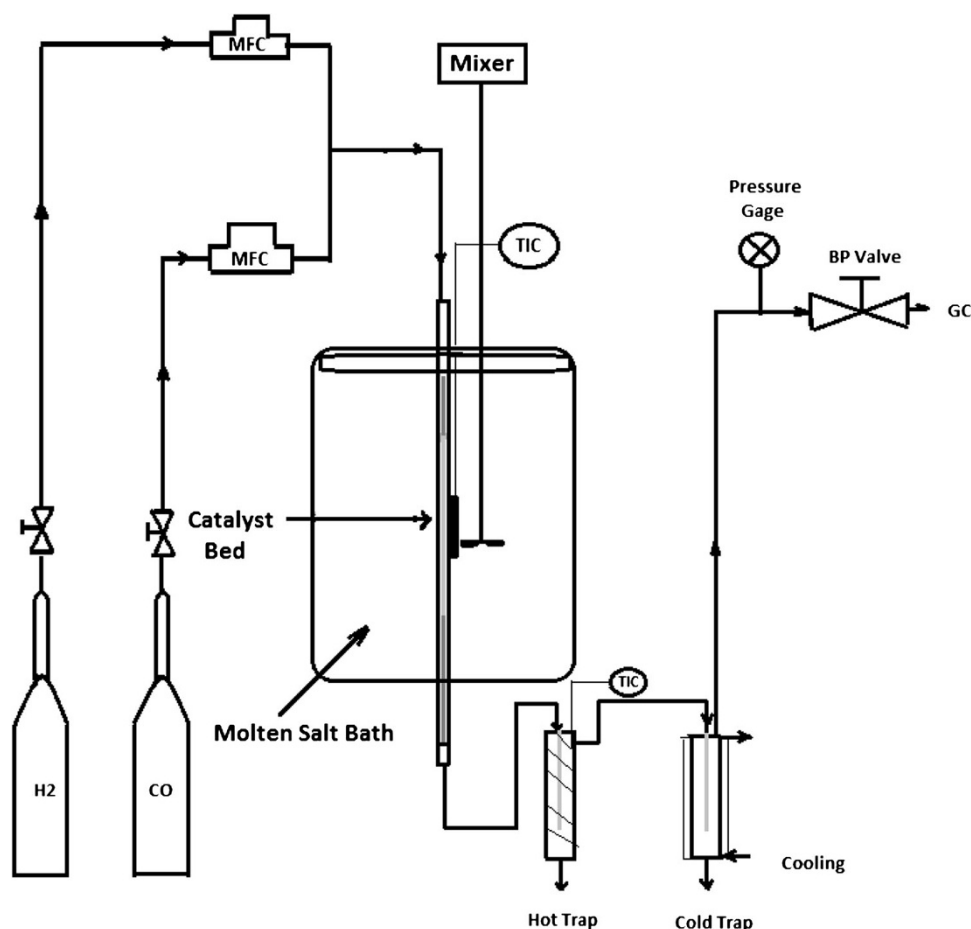
$$\%D_{\text{Total Co}} = \frac{H_2 \text{ uptake} \times \text{atomic weight} \times \text{stoichiometry}}{\%\text{Metal}}$$
$$= \frac{\text{Number of Co}^o \text{ atoms on the surface} \times 100}{\text{Total number of Co}^o \text{ atom}} \tag{3}$$

$$\%D_{\text{reduced Co}} = \frac{\text{Number of Co}^o \text{ atoms on the surface} \times 100}{\text{Total number of Co}^o \text{ atom} \times \text{Reduced fraction}} \tag{4}$$

$$O_2 \text{uptake (moles/g}_{cat})$$
$$= \frac{\text{Sum of consumed pulses areas} \times \text{calibration value}}{\text{Sample weight} \times 24.5} \tag{5}$$

Fig. 11 Experimental setup

Reduced fraction

$$= \frac{O_2 \text{ uptake (moles/g cat)} \times 2/3 \times \text{atomic weight}}{\text{Percentage metal}} \quad (6)$$

Diameter $(nm)_{total \, Co}$

$$= \frac{6{,}000}{\text{Density} \times \text{maximum area} \times \text{dispersion}} \quad (7)$$

Diameter $(nm)_{reduced \, Co}$

$$= \frac{6{,}000}{\text{Density} \times \text{maximum area} \times \text{dispersion} \times \text{Reduced fraction}} \quad (8)$$

Reaction testing

Fischer–Tropsch synthesis has been performed in a tubular down-flow, fixed-bed reactor system. Figure 11 shows the experimental setup. The reactor was made up of stainless steel tube of 450-mm length and 22-mm inside diameter. Brooks's 5850 mass flow controllers were used to add H_2 and CO at the desired rate to the reactor. Typically, 1 g of the catalyst was charged into the reactor. The reactor was placed in a molten salt bath with a stirrer to ensure a uniform temperature along the catalytic bed. The bath temperature was controlled via a PID temperature controller. The catalyst reduced under flowing of hydrogen at 400 °C for 12 h. After the catalyst reduction, the mixed gases (CO and H_2) were fed at a flow of 50 ml/min, a temperature of 220 °C, H_2/CO ratio of 2 and pressure of 2 MPa. The products were continuously removed from the reactor and passed through two traps, one maintained at 100 °C (hot trap) and the other at 0 °C (cold trap). The CO, CO_2 and other gaseous products were monitored with time intervals of 2 h. The liquid products were collected after completion of the run and analyzed by means of three gas chromatographs, a Shimadzu 4C gas chromatograph (Shimadzu Corp., Kyoto, Japan) equipped with two subsequent connected packed columns: Porapak Q (Sigma-Aldrich Corp., St. Louis, MO, USA) and molecular sieve 5Å, and a TCD with argon which was used as a carrier gas for hydrogen analysis. A Varian CP 3800 with a Petrocol Tm DH100 fused silica capillary column (Sigma-Aldrich Corp., St. Louis, MO, USA) and a flame ionization detector (FID) were used for liquid products so that a complete product distribution could be provided. A Varian CP 3800 with a chromosorb column and a TCD was used for CO, CO_2, CH_4 and other non-condensable gases.

Conclusions

Ruthenium-promoted cobalt nanocatalysts supported on CNTs are prepared using microemulsion technique with water-to-surfactant ratios of 0.5–1.5 and their physicochemical properties and performance in FTS have been assessed and were compared with the catalyst prepared by impregnation method. Ruthenium increased the percentage reduction of the unpromoted catalyst by a factor of 25 %. Very narrow particle size distribution has been produced by the microemulsion technique at the relatively high loadings of active metals (15 wt% Co and 1 wt% of Ru). Addition of ruthenium increased the percentage conversion and C_5^+ selectivity of the unpromoted catalyst by a factor of 22.6 and 7 %, respectively. Using microemulsion technique with water-to-surfactant ratio of 0.5 decreased the average cobalt oxide particle sizes to 4.8 nm. The %dispersion is almost doubled and the %reduction increased by 28 %. Activity and selectivity were found to be dependent on the catalyst preparation method and cobalt average particle sizes. The percentage of CO conversion and FTS rate increased from 59.09 to 75.05 % and 0.291 to 0.372 g HC/g cat/h), respectively, while the C_5^+ liquid hydrocarbons selectivity decreased slightly.

Authors' information Ahmad Tavasoli: professor, university of Tehran. Somaye Taghavi: masterstudent, university of Tehran. Saber Tabyar: master student. Saba karimi:master of student, university of Tehran.

References

1. Dry ME (2002) The Fischer–Tropsch process. Catal Today 71:227–241
2. Van Der Laan GP, Beenackers A (2000) Appl Catal A 193:39–53
3. Iglesia E (1997) Design, synthesis, and use of cobalt-based Fischer–Tropsch synthesis catalysts. Appl Catal A 161:59–78
4. Trepanier M, Tavasoli A, Dalai AK, Abatzoglou N (2009) Co, Ru and K loadings effects on the activity and selectivity of carbon nanotubes supported cobalt catalyst in Fischer–Tropsch synthesis. Appl Catal A 353:193–202
5. Jacobs G, Das TK, Zhang Y, Li J, Racoillet G, Davis BH (2002) Fischer–Tropsch synthesis: support, loading, and promoter effects on the reducibility of cobalt catalysts. Appl Catal A 233:263–281
6. Eriksson S, Nylén U, Rojas S, Boutonnet M (2004) Preparation of catalysts from microemulsions and their applications in heterogeneous catalysis. Appl Catal A 265:207–219
7. Paul BK, Moulik SP (1997) Microemulsions: an overview. Dispers Sci Tech 18:301–367
8. Boutonnet M, Lögdberg S, Svensson EE (2008) Recent developments in the application of nanoparticles prepared from w/o microemulsions in heterogeneous catalysis. Curr Opin Colloid Interface Sci 13:270–286
9. Jacobs G, Das TK, Zhang Y, Li J, Racoillet G, Davis BH (2002) Fischer–Tropsch synthesis: support, loading, and promoter effects on the reducibility of cobalt catalysts. Appl Catal A Gen 233:263–281
10. Berge VPJ, van de Loosdrecgt J, Barradas S, van der Kraan AM (2000) Oxidation of cobalt based Fischer–Tropsch catalysts as a deactivation mechanism. Catal Today 58:321–334
11. Reuel RC, Bartholomew CH (1984) Effects of support and dispersion on the CO hydrogenation activity/selectivity properties of cobalt. J Catal 85:78–88
12. Das TK, Jacobs G, Patterson PM, Conner WA, Li J, Davis BH (2003) Fischer–Tropsch synthesis: characterization and catalytic properties of rhenium promoted cobalt alumina catalysts. Fuel 82:805–815
13. Martinez A, Prieto G (2007) Breaking the dispersion-reducibility dependence in oxide-supported cobalt nanoparticles. J Catal 245:245–470
14. Bechera R, Balloy D, Vanhove D (2001) Catalytic properties of Co/Al_2O_3 system for hydrocarbon synthesis. Appl Catal A 207:343–353
15. Elbashir NO, Roberts CB (2005) Enhanced incorporations of α-olefins in the Fischer–Tropsch synthesis chain-growth process over an alumina supported cobalt catalysts in near-critical and supercritical hexane medium. Ind Eng Chem Res 44:505–521
16. Tavasoli A, Mortazavi Y, Khodadadi A, Sadagiani K (2005) Effects of different loadings of Ru and Re on physico-chemical properties and performance of 15% Co/Al_2O_3 FTS catalysts. Iranian J Chem Chem Eng 35:9–15
17. Tavasoli A, Sadaghiani K, Nakhaeipour A, Ghalbi Ahangari M (2007) Cobalt loading effects on the structure and activity for Fischer–Tropsch and water–gas shift reactions of $Co/Al2O3$ catalysts. IJCCE 29:1–12
18. Tavasoli A, Sadagiania K, Khorashe F, Seifkordi AA, Rohania AA, Nakhaeipour AA (2008) Cobalt supported on carbon nanotubes—a promising novel Fischer–Tropsch synthesis catalyst. Fuel Process Technol 89:491–498
19. Tavasoli A, Malek Abbaslou R, Trepanier M, Dalai AK (2008) Fischer–Tropsch synthesis over cobalt catalyst supported on carbon nanotubes in a slurry reactor. Appl Catal A 345:134–142
20. Chen W, Fan Z, Pan X, Bao X (2008) Effect of confinement in carbon nanotubes on the activity Fischer–Tropsch iron catalysts. J Am Chem Soc 130:9414–9419